In silico screening against wild-type and mutant *Plasmodium falciparum* dihydrofolate reductase

Gary B. Fogel [a], Mars Cheung [a], Eric Pittman [b], David Hecht [b],*

[a] *Natural Selection Inc., 9330 Scranton Road, Suite 150, San Diego, CA 92121, USA*
[b] *Southwestern College, 900 Otay Lakes Road, Chula Vista, CA 91910, USA*

Abstract

Modeling studies were performed on known inhibitors of wild-type as well as quadruple mutant *Plasmodium falciparum* dihydrofolate reductase (DHFR). GOLD was used to dock 31 pyrimethamine derivatives into the active site of DHFR obtained from the X-ray crystal structures 1J3I.pdb and 1J3K.pdb. Predicted binding affinities from a scoring function were analyzed and evaluated in order to develop criteria for selecting compounds having a greater chance of activity versus wild-type and resistant strains of *P. falciparum* for future high-throughput screening experiments.
© 2007 Elsevier Inc. All rights reserved.

1. Introduction

In recent years, there has been an alarming emergence of drug-resistant strains of bacteria, viruses, and parasites. These include: methicillin-resistant *Staphylococcus aureus* (MRSA), vancomycin/glycopeptide-intermediate *S. aureus* (VISA/GISA), *Streptococcus pneumoniae*, vancomycin-resistant enterococci (VRE), human immunodeficiency virus (HIV), and *Plasmodium* [1]. Even as new therapeutics are developed, these organisms have the potential to rapidly evolve and regain resistance. The evolution of multiple resistant strains of pathogens demands not only immediate proper diagnosis and treatment but requires a more effective drug development strategy.

Traditional drug discovery follows a common dogma: one protein per target, one target per drug. Recent advances in systems biology arising from our increased understanding of gene expression profiles, pathways, protein translation, and postprocessing, have caused some researchers to question this approach in support of a method to design and develop drugs that are effective simultaneously against multiple targets [2–4].

Some successful applications of this approach include: anti-apoptotic pan-caspase inhibitors for HBV and HCV [5], cancer [6], Alzheimer's disease [7], as well as the development of promiscuous tyrosine kinase inhibitors and G-protein receptor antagonists for cardiovascular disease [8].

This approach shows promise for addressing drug resistance that arises through the evolution and diversification of targets. For example, as a protein target adapts in response to drug therapy, a multi-targeted drug may still retain the ability to inhibit activity of mutant protein targets. The key to this strategy is to identify and develop compounds that bind with high affinity to different active sites and/or binding sites simultaneously.

Malaria provides an ideal model system to evaluate this strategy. In the case of two of the most prevalent malaria strains, *Plasmodium falciparum* (*Pf*) and *P. vivax* (*Pv*), clinical resistance arises from key amino acid substitutions in the target protein. These strains of malaria have developed resistance to anti-folate compounds such as pyrimethamine and cycloguanil that target dihydrofolate reductase (DHFR)–thymidylate synthetase [9–11]. Resistance arises from amino acid substitutions in *Pf*-DHFR at residues 51, 59, 108 and 164 and *Pv*-DHFR at residues 58, 117, and 173 [12–14].

Additionally, there is a wealth of structure–activity relationship (SAR) data in malaria in the literature. Structure-based

---

* Corresponding author. Tel.: +1 619 421 6700; fax: +1 619 482 6503.
E-mail address: dhecht@swccd.edu (D. Hecht).

drug design and discovery has been employed to improve the efficiency and productivity of new-leads discovery efforts for anti-malarials [15,16]. These efforts include X-ray crystallography [12,14], molecular modeling [17], and quantitative structure–activity relationships (QSAR) [18–27]. From these efforts, a third generation anti-folate active compound (WR99210) in resistant strains of both *Pf* and *Pv*, was discovered [28].

In this study, we present a methodology employing *in silico* protein–ligand docking and scoring algorithms for identifying inhibitors active simultaneously against wild-type (WT) and mutant forms of *Pf*-DHFR. This methodology is designed to filter small molecule libraries based on predicted relative binding affinity and to generate a small, "focused,"

compound screening library enriched with dual inhibitors. Additionally, this approach provides models of the predicted binding mode(s) and conformation(s) in an active site that can be useful in the generation and evaluation of SAR hypotheses.
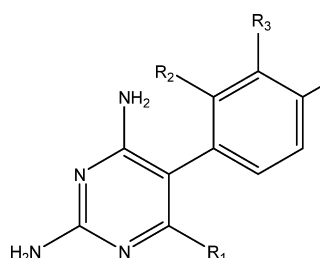
2. Materials and methods

2.1. Docking protocols

The X-ray crystal structures of both *Pf* WT DHFR–TS (1J3I.pdb) [12] and quadruple mutant DHFR–TS (1J3K.pdb) [12] were identified for these studies. Both of these structures contain the third-generation *Pf*-DHFR inhibitor WR99210

Table 1
Structures, experimental pK_i values and docking scores are listed [18,19]

ID	R_1	R_2	R_3	R_4	pK_{iWT}(nM) [18,19]	pK_{iMut} (nM) [18,19]	Protein–ligand score (WT)	Protein–ligand score (Mut)
P39	$-C_6H_{13}$	H	H	H	9.52	8.85	−97.57	−105.21
P40	$-(CH_2)_2O(CH_2)_3OC_6H_5$	H	Cl	H	9.40	8.77	*−136.08*	*−130.61*
P32	$-(CH_2)_3C_6H_4-(p\text{-}OCH_3)$	H	Cl	H	8.66	8.70	*−115.14*	*−107.94*
P31	$-(CH_2)_3C_6H_5$	H	Cl	H	8.92	8.70	*−124.93*	*−108.72*
P29	$-(CH_2)_3COOCH_3$	H	Cl	H	9.30	8.57	*−110.73*	*−103.00*
P30	$-CH_2CH_3$	H	Cl	H	9.10	8.48	−96.77	−90.93
P43	$-(CH_2)_3OCOC_6H_5$	H	Cl	H	8.82	8.44	*−127.66*	*−117.77*
P44	$-(CH_2)_3OCOOCH_2C_6H_5$	H	Cl	H	8.92	8.44	*−144.47*	*−126.37*
P33	$-(CH_2)_3C_6H_5$	H	H	H	9.30	8.33	*−109.87*	*−113.89*
P47	$-(CH_2)_3OCOC_6H_5$	H	H	H	8.47	7.85	*−130.95*	*−119.05*
P38	$-CH_3$	H	Cl	H	8.72	7.85	−91.81	−84.39
P26	$-(CH_2)_3COOCH_3$	H	H	H	9.22	7.62	*−103.39*	*−105.85*
P42	$-(CH_2)_3OCOCH_3$	H	Cl	H	8.51	7.50	*−110.62*	*−103.05*
P20	$-CH_2CH_3$	H	H	H	8.64	7.50	−93.09	−88.75
P13	$-CH_2CH_3$	H	Cl	Cl	9.00	7.27	−96.22	−83.82
P41	$-(CH_2)_3OH$	H	Cl	H	8.04	7.24	−113.73	−91.47
P12	$-(CH_2)_3C_6H_5$	H	H	Cl	9.15	6.77	−118.58	−87.58
P46	$-(CH_2)_3OCOCH_3$	H	H	H	7.97	6.63	−102.20	−98.12
P15	$-CH_2CH_3$	H	$R_3\text{-}OCH_2O\text{-}R_4$		8.96	6.57	−97.93	−87.31
P17	$-CH_2CH_3$	H	H	$-CH_3$	9.40	6.55	−92.72	−85.35
P21	$-CH_2CH_3$	H	H	Br	9.52	6.52	−92.25	−80.45
P7	$-CH_2CH_2CH_3$	H	H	Cl	9.30	6.44	−100.75	−90.32
P16	$-(CH_2)_3COOCH_3$	H	H	Cl	9.52	6.44	−103.77	−93.83
Pyrimidine	$-CH_2CH_3$	H	H	Cl	9.52	6.41	−95.77	−81.57
P2	$-CH(CH_3)_2$	H	H	Cl	9.52	6.27	−97.27	−84.65
P45	$-CH_2OH$	H	H	H	7.07	6.26	−111.26	−85.62
P18	$-CH_2CH_3$	H	H	OCH_3	9.05	6.21	−92.23	−87.31
P3	$-CH_2CH(CH_3)_2$	H	H	Cl	9.52	6.10	−95.07	NA*
P5	$-C_6H_4-(p\text{-}OCH_3)$	H	H	Cl	8.37	5.80	−100.12	NA*
P14	$-CH_2CH_3$	Cl	H	Cl	7.90	5.73	−67.73	−68.04
P4	$-C_6H_5$	H	H	Cl	8.54	5.46	−88.76	NA*

Bold and italicized values in the ID column represent compounds identified as active against both WT and mutant forms of *Pf*-DHFR. Compounds with unrealistic poses were considered inactive and are indicated with an asterisk in the protein–ligand score column.

bound to the active site in the presence of NADPH, and are assumed to be representative of bound conformations *in vivo*.

To simplify docking calculations, DHFR structures were truncated to a 10 Å radius from each atom in the bound WR99210 inhibitor using Deepview (Swiss-PDBviewer) [29]. The inhibitor WR99210 was then removed, and the *.pdb files were imported into Molecular Operating Environment (MOE) [30]. The ''wash'' function in MOE was used to refine the structures including addition of explicit hydrogen atoms. Lastly, the protein structures were exported as *.pdb files for input into Genetic Optimization for Ligand Docking (GOLD) [31].

Thirty-one compounds with experimentally derived wild-type as well as quadruple mutant *Pf*-DHFR pK_i values were obtained from the literature [18,19] (Table 1). All compounds were drawn using Chemdraw (Cambridgesoft Inc.) [32] and then imported into MOE. The two-dimensional structures were ''washed,'' converted to three dimensions, and minimized using the MMFF94x [33] gas phase potential. The structures were finally exported in *.sdf format for use with GOLD.

Docking experiments were performed using the default GOLD fitness function (VDW = 4.0, H-bonding = 2.5) and default evolutionary parameters: population size = 100; selection pressure = 1.1; # operations = 100,000; # islands = 5; niche size = 2; migration = 10; mutation = 95; crossover = 95 [31]. The carbonyl oxygen on Leu 164 (for 1J3K.pdb) and Ile 164 (for WT 1J3I.pdb) were selected as the binding site centers for all calculations. Fifty docking runs were performed per structure unless 3 of the 50 poses were within 1.5 Å rmsd of each other. All poses were output into a single *.sdf file. A single desktop computer operating with WinXP Media edition (AMD 3800+, 64 bit processor (~2.65 GHz) and 1 GB RAM) processed 25 compounds in ~3 h.

The output from GOLD was imported into Molegro Virtual Docker (Molegro ApS) [34] for scoring. We previously evaluated several different scoring functions and selected the protein–ligand interaction score from Molegro [35].

2.2. Pose validation and evaluation

In order to verify that poses resulting from *in silico* docking represent correctly bound conformations, each pose was visually inspected and compared to the experimentally determined binding modes and conformations of WR99210. Key protein–ligand contacts and interactions were examined. These included hydrogen bonding interactions with Asp 54, Ile 14, and potentially Leu or Ile 164 as well as potential interactions with Ile 112 and Pro 113 [12–14].

Much of the resistance of the mutant strains of *Pf* and *Pv* can be attributed to steric clashes of bound compounds with Asn 108 (mutated from Ser 108) as well as subtle shifts in the positioning of residue Ile 164 (mutated from Leu 164) [12–14]. Compound WR99210 was designed to avoid this steric clash with Asn 108 through the introduction of a flexible 3-carbon connector between the two aromatic rings [28] (Fig. 1).

As WR99210 was used for evaluating and selecting poses, we first verified experimentally determined bound conforma-

tions using *in silico* methods. For this purpose, WR99210 was docked into the active site of wild-type *Pf*-DHFR–TS crystal structure (1J3I.pdb) as well as the active site of the quadruple mutant crystal structure (1J3K.pdb). The resulting docked conformations of WR99210 (to both wild-type and quadruple mutant X-ray crystal structures) fell within 1.1 Å rmsd for all atoms from the bound X-ray conformations (Fig. 1) [35].

In many cases the compounds did not converge during docking because of large and flexible R-groups. The resulting poses were considered unrealistic when compared to the bound X-ray structure conformations of WR99210 due to: loss of key hydrogen bonds to Asp 54 and Ile 14; non-superimposition of the diaminopyrimidine ring onto WR99210; as well as unfavorable steric clashes with Asn 108. For this reason, visual inspection of all poses was then performed to eliminate poses considered inconsistent with the bound WR99210 X-ray conformation. Only the top scoring (GOLD score) pose was retained and scored. For several compounds, all docked poses were considered inconsistent with respect to the bound
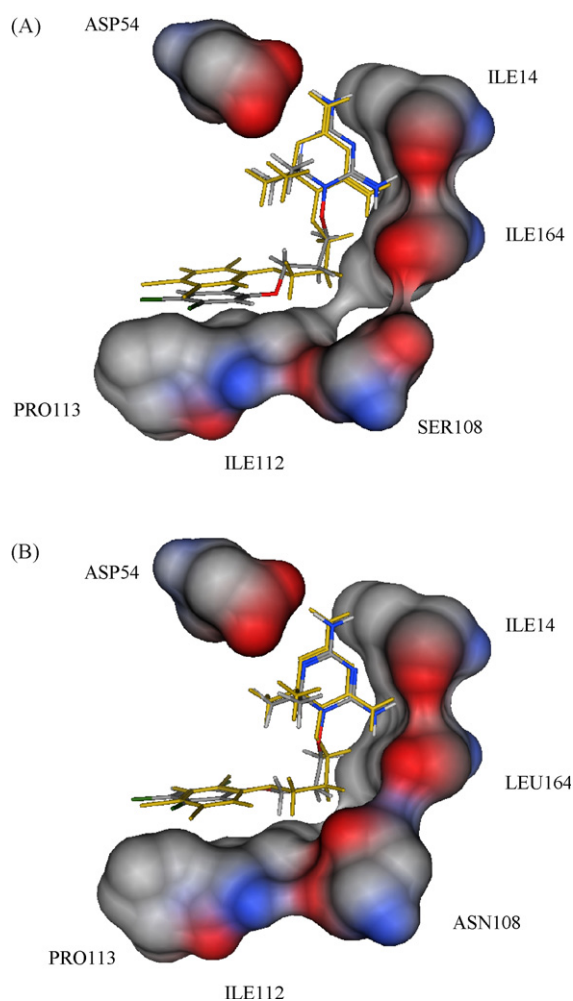

Fig. 1. Superposition of bound X-ray crystal of WR99210 vs. conformations from docking experiments. (A) WR99210 from WT *Pf*-DHFR–TS (1J3I.pdb) in GOLD and the docked conformation in CPK, rmsd = 1.095 Å [35]. (B) WR99210 from quadruple mutant *Pf*-DHFR–TS (1J3K.pdb) in GOLD and the docked conformation in CPK rmsd = 0.951 Å [35].
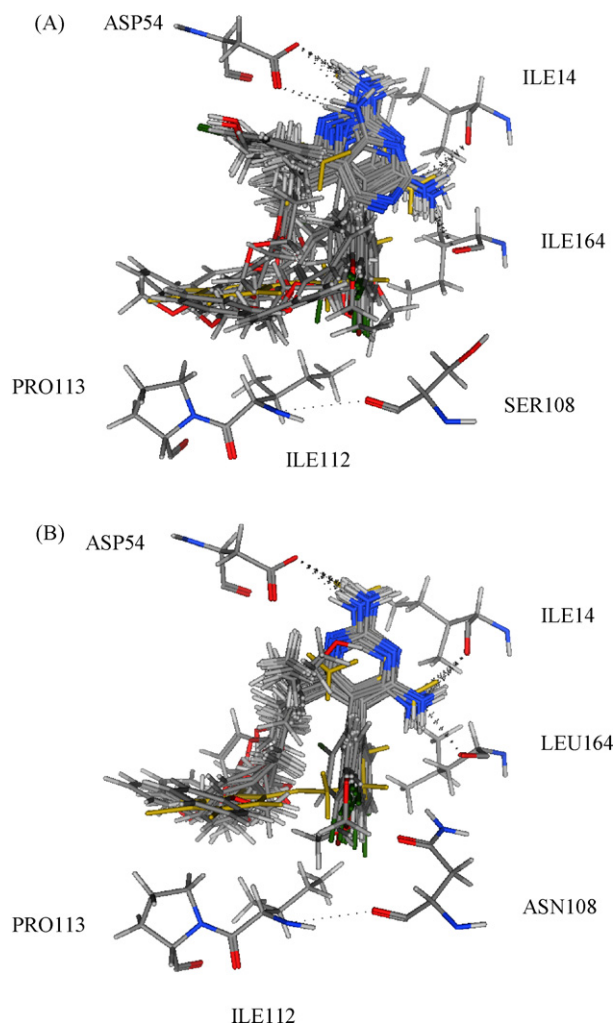
Fig. 2. Superposition of all docked poses on the bound X-ray crystal of WR99210. (A) WR99210 from WT Pf-DHFR–TS (1J31.pdb) in GOLD and 31 docked compounds [18,19] in CPK. (B) WR99210 from quadruple mutant Pf-DHFR–TS (1J3K.pdb) in GOLD and 28 docked compounds [18,19] in CPK.
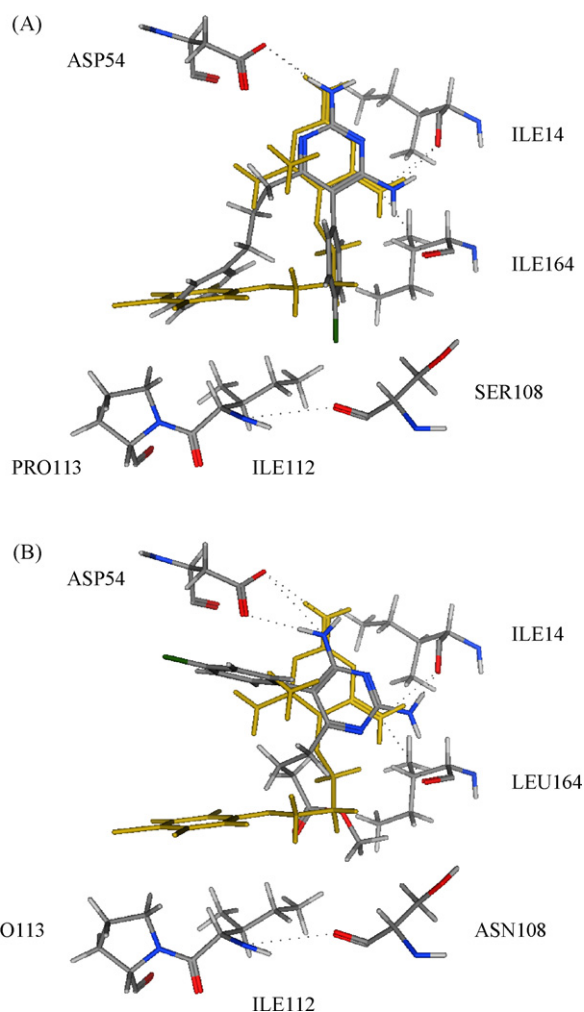

Fig. 3. Superposition of docked poses on the bound X-ray crystal of WR99210 illustrating the two different observed binding modes. (A) The standard binding mode. WR99210 from WT Pf-DHFR–TS (1J31.pdb) in GOLD and P12 [18,19] in CPK. (B) The alternative binding mode. WR99210 from quadruple mutant Pf-DHFR–TS (1J3K.pdb) in GOLD and P16 [18,19] in CPK.

WR99210 conformation. These compounds were considered "inactive" and given a value of "N/A" in Table 1.

3. Results

Fig. 2 illustrates the superposition of the top scoring poses from 31 compounds with WR99210 from the WT DHFR

docking experiments as well as the superposition of 28 compounds versus WR99210 from the mutant DHFR docking experiments. Note that three compounds docked versus the mutant DHFR did not converge and/or did not give reasonable poses and were scored as inactive.

Fig. 2 also illustrates that there were at least two different clusters of binding modes identified from the WT DHFR
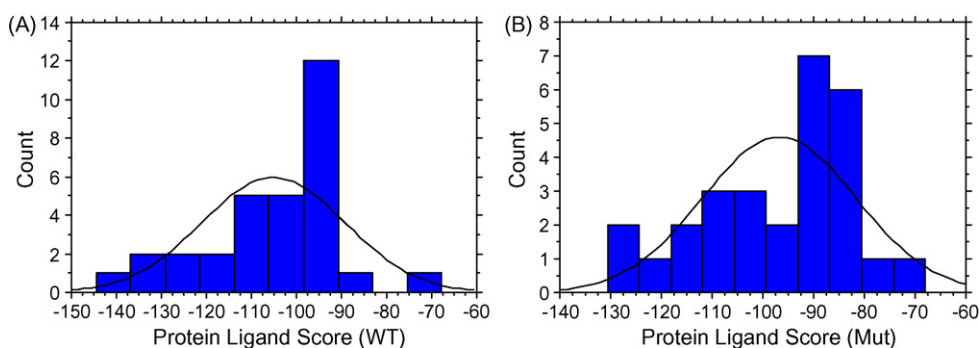

Fig. 4. (A) Distribution of WT protein–ligand interaction scores. (B) Distribution of mutant protein–ligand interaction scores.

experiments but only one identified from the mutant DHFR docking experiments. Compounds P12 and P16 shown in Fig. 3 are representative of these two binding modes. While compound P12 is consistent with the binding mode of compound WR99210 (making similar protein–ligand contacts and interactions), the docked diaminopyrimidine ring of compound P16 is rotated 90°. Despite this difference in orientation, the P16 pose maintains H-bonds with Asp 54, Ile 14, and potentially Ile 164.

This second binding mode may reflect an artifact of the inflexibility of the binding site during the docking experiments, a well-recognized limitation of many docking algorithms. The compound was rotated in order to avoid steric clashes with Ser 108 and Ile 164. However, these experiments may indicate an alternative binding mode. This alternative binding mode was also present in the top scoring poses for compounds P4, P5, P33, P39, and P46.

Close examination of individual poses for each compound did not reveal a significant impact of these two different binding modes upon the resulting docking scores (data not shown). For the very practical purpose of implementing this methodology for screening and focused library generation and in lieu of structural data to the contrary, the poses with the alternative binding mode were retained and scored. Table 1 presents the structures with pK_i (WT) and pK_i (Mut) values [18,19]. Also listed are the docking scores for these 31 compounds [35].

The distribution of protein ligand scores for both the WT and quadruple mutant are broadly similar in nature, with clusters of samples in the range [−90,−100] (Fig. 4). However, a two-sample Kolmogorov–Smirnov test suggests that the null hypothesis of distribution equivalency should be rejected ($D = 0.4712$, p-value = 0.0029). This is likely to be a reflection of differences in the relative binding affinities of each compound for these two DHFR targets. This observation is consistent with the fact that almost two thirds of the compounds lost significant (greater than 10–100-fold) potency versus the mutant form of DHFR.

4. Discussion

4.1. Docking score analysis

Perhaps the greatest weakness in the application of *in silico* screening for new lead discovery is the well-documented difficulty of correlating docking scores with binding affinities and/or inhibitory activities [36,37]. This is surprising and especially frustrating given that docking algorithms can successfully predict the bound conformations of a ligand down to <1 Å rmsd of the experimentally determined bound conformation (as presented for compound WR99210).

Previously, we presented a comparison of several scoring functions calculated from poses of the 31 pyrimethamine analogues [35]. The best linear correlation to mutant *Pf*-DHFR pK_i was 0.68. Unfortunately, as all of the compounds were potent against WT *Pf*-DHFR, it was not possible to calculate linear the correlation of their docking scores with their pK_i values (Table 1).

Table 2
Confusion matrix for dual activity

Actual	Predicted	
	Active	Inactive
Active	10	4
Inactive	0	17

The overall goal of developing this screening methodology is to select focused screening libraries having enhanced hit rates simultaneously for both wild-type and mutant forms of an enzyme target. As the activities of any hits resulting from an *in silico* screen need to be verified experimentally, it is far more important to be able to select actives with a minimum of false positives than it is to very accurately rank the relative activities of the active compounds.

From an analysis of the docking scores, a docking score of −100 (corresponding to pK_i of 32 nM or less) was selected as a threshold for a determination of activity or inactivity. Fourteen compounds listed in Table 1 have pK_i values ≥7.5 for both the WT and mutant forms of DHFR. From the docking scores, 10 of these were correctly identified as ''active'' making the overall hit-rate accuracy for identifying for dual-activity inhibitors from this analysis ∼71%. All ''inactive'' compounds were correctly classified. The confusion matrix for dual activity is presented in Table 2.

4.2. Focused screening library generation

A commonly used estimate of true actives present in a typical commercially available screening library is 1%. Thus, a library containing 100,000 compounds will contain 1000 true actives. Given no false positives and assuming the same accuracy for predicting actives as presented here for this small series of pyrimethamine analogues holds for larger datasets, this *in silico* screen would result in a focused library of 710 compounds active against both WT and mutant forms of *Pf*-DHFR.

As this study focused on a small set of structurally similar pyrimethamine analogues the analysis probably reflects a ''best-case'' scenario. Additional structure classes and more diverse sets of compounds will likely decrease the true positive accuracy. Even so, this approach shows promise and potential for future screens against multiple targets.

4.3. Structure–activity relationships

In addition to predicted relative binding/inhibition activities discussed above, these studies provide predicted binding modes and protein–ligand interactions that can be useful in development of SAR models. SAR models are critical for the eventual development of novel inhibitors of both wild-type and mutant *Plasmodium* DHFR.

Several trends are obvious from an analysis of the R-groups and pK_i (Mut) values presented in Table 1. First, when R_4 is a Cl or another bulky group, the compound tends to be inactive
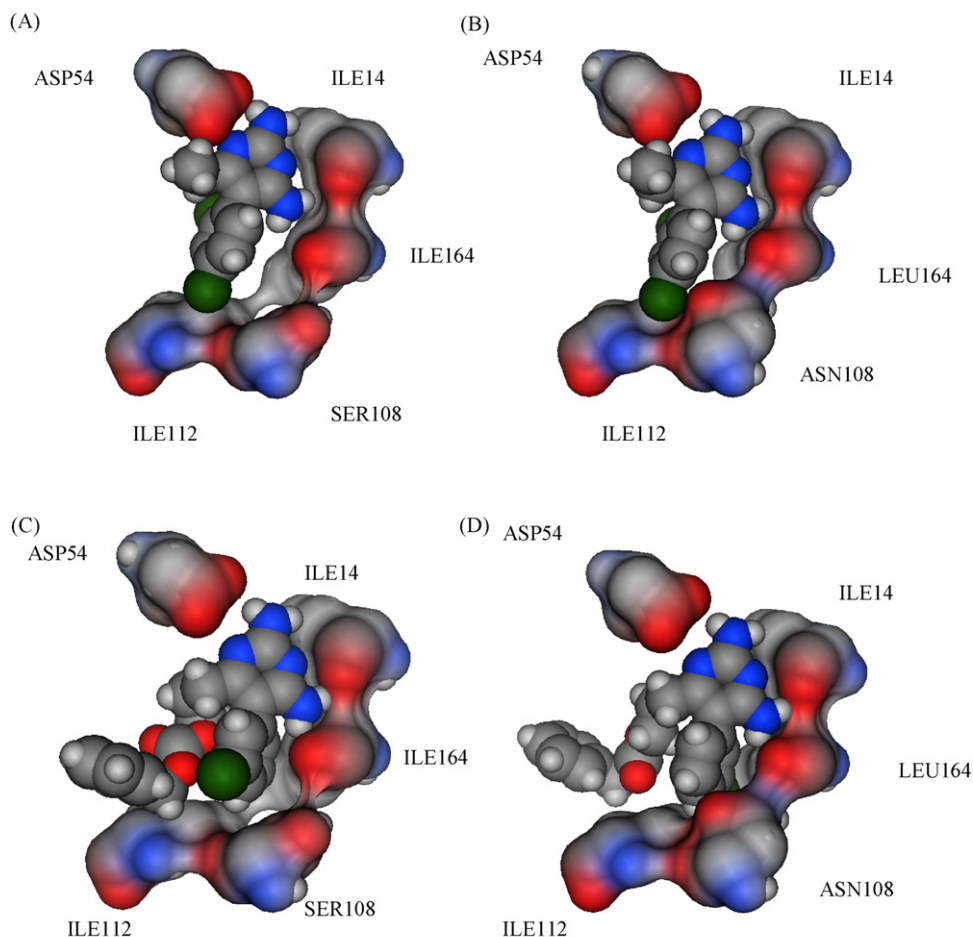
Fig. 5. Predicted key protein–ligand contacts and conformations of bound (A) P14 to wild-type *Pf*-DHFR (1J3I.pdb), (B) P14 to quadruple mutant *Pf*-DHFR (1J3K.pdb), (C) P44 to wild-type *Pf*-DHFR (1J3I.pdb) and (D) P44 to quadruple mutant *Pf*-DHFR (1J3K.pdb).

versus mutant DHFR. R_4 corresponds to the *para*-position on the second aromatic ring. Secondly, when R_3 is Cl or another bulky group the compound often retains activity. The R_3 position corresponds to the *meta*-position on the second aromatic ring. Lastly, when R_1 is a long chain with multiple oxygens, the compounds retain activity.

An analysis of predicted protein–ligand interactions from the docked poses was performed in order to understand the structural origins of these trends. For purposes of illustration, compound P14 ($pK_{iWT} = 7.90$ and $pK_{imutant} = 5.73$) having a Cl at position R_4 and a short hydrocarbon chain in position R_1 and compound P44 ($pK_{iWT} = 8.92$ and $pK_{imutant} = 8.44$) having a Cl in the R_3 position and a long chain in the R_1 position were used. Both compounds fit the observed SAR trend with compound P14 losing substantial activity and compound P44 retaining significant activity versus mutant *Pf*-DHFR.

Analysis of key protein–ligand contacts from the poses provides insight into the retained activity for compound P44 and loss of activity for compound P14. As seen in Fig. 5, both P14 and P44 fit nicely in the wild-type DHFR binding. However, in the mutant DHFR binding site, the *para*-chlorine from P14 clashes with Asn 108 and is potentially a source for its

poor binding. Interestingly, the *meta*-chlorine on compound P44 avoids this steric clash by rotating 180° in the mutant binding site.

Both ligands appear to have potential H-bond interactions with Asp 54, Ile 14, and Leu 164. Additionally, the long chain in the R_1 position of compound P44 appears to increase favorable interactions with Ile 112 and Pro 113 in a manner similar to WR99210.

These observations support the SAR trends generated from Table 1 and provide detailed structural insight into their origins. The understanding and knowledge arising from analyses such as these will be extremely useful in the future design and development of novel DHFR inhibitors.

5. Conclusions

In response to the increase of resistant pathogens as well as to our rapidly increasing understanding of systems biology and metabolic pathways there has recently been a renewed interest in discovering and developing multi-target drugs [2–4]. Recent successes have successfully integrated structure-based drug design and discovery with screening, SAR and lead optimization approaches [5–8,28]. To fully meet this challenge, new

tools and approaches for drug discovery and development are required.

Focused compound screening libraries are commonly used to improve the efficiency and productivity of early drug discovery efforts. Traditionally each compound in a focused library is selected based upon structural and physical properties that will increase its probability of having activity for one specific target. In this paper we have extended this approach in order to identify potential multi-target inhibitors.

Modeling studies were performed with known inhibitors of the wild-type and quadruple mutant forms of Pf-DHFR. A predictive model of relative inhibition and binding affinities for anti-malarial compounds against two protein targets was developed. Using this model, compounds active against both can be selected as candidates for future experimental studies. In addition, the docked poses (resulting from these studies) provide details of the predicted binding mode(s) and the key molecular interactions. These will provide opportunities for medicinal chemists to generate testable SAR hypotheses for lead optimization and development. The approach was first tested on known DHFR inhibitors in order to refine and validate the methodology before application to other aspects of anti-malarial drug discovery and possibly even other targets and diseases.

Acknowledgements

Appendix A. Supplementary data

Supplementary data associated with this article can be found, in the online version, at doi:10.1016/j.jmgm.2007.10.006.

References

[1] National Center for Disease Control, Internet References, 2007 Retrieved from http://www.cdc.gov/drugresistance/about.htm (July 27, 2007).

[2] G.R. Zimmermann, J. Lehár, C.T. Keith, Multi-target therapeutics: when the whole is greater than the sum of the parts, Drug Discov. Today 12 (2007) 24–42.

[3] P. Csermely, V. Ágoston, P. Sándor, The efficiency of multi-target drugs: the network approach might help drug design, Trends Pharmacol. Sci. 26 (2005) 178–182.

[4] R. Morphy, Z. Rankovic, fragments, network biology and designing multiple ligands, Drug Discov. Today 12 (2007) 156–160.

[5] P.J. Pockros, E.R. Schiff, M.L. Shiffman, J.G. McHutchison, R.G. Gish, N.H. Afdhal, M. Makhviladze, M. Huyghe, D. Hecht, T. Oltersdorf, D.A. Shapiro, Oral IDN-6556, an anti-apoptotic caspase inhibitor, lowers aminotransferases in patients with chronic hepatitis C, Hepatology 46 (2007) 324–329.

[6] T. Hampton, "Promiscuous" anticancer drugs that hit multiple targets may thwart resistance, JAMA 292 (2004) 419–420.

[7] Z. Hong-Yu, One-compound-multiple-targets strategy to combat Alzheimer's disease, FEBS Lett. 579 (2005) 5260–5264.

[8] C. Flordellis, P. Papathanasopoulos, A. Lymperopoulos, J. Matsoukas, H. Paris, Emerging therapeutic approaches multi-targeting receptor tyrosine kinases and G protein-coupled receptors in cardiovascular disease, Cardiovas. Hematol. Agents Med. Chem. 5 (2007) 133–145.

[9] J.E. Hyde, Mechanisms of resistance of Plasmodium falciparum to antimalarial drugs, Microbes Infect. 4 (2002) 165–174.

[10] Y. Yuthavong, Basis for antifolate action and resistance in malaria, Microbes Infect. 4 (2002) 175–182.

[11] R. Ferone, Folate metabolism in malaria, Bull. World Health Organ. 55 (1977) 291–298.

[12] J. Yuvaniyama, P. Chitnumsub, S. Kamchonwongpaison, J. Vanichtanankul, W. Sirawaraporn, P. Taylor, M. Walkinshaw, Y. Yuthavong, Insights into antifolate resistance from malarial DHFR–TS structures, Nat. Struct. Biol. 10 (2003) 357–365.

[13] W. Sirawaraporn, T. Sathikul, R. Sirawaraporn, Y. Yuthavong, D.V. Santi, Antifolate-resistant mutants of Plasmodium falciparum dihydrofolate reductase, Proc. Natl. Acad. Sci. 94 (1997) 1124–1129.

[14] P. Kongsaeree, P. Khongsuk, U. Leartsakulpanich, P. Chitnumsub, B. Tarnchombpoo, M.D. Walkinshaw, Y. Yuthavong, Crystal structure of dihydrofolate reductase from Plasmodium vivax: pyrimethamine displacement linked with mutation-induced resistance, Proc. Natl. Acad. Sci. U.S.A. 102 (2005) 13046–13051.

[15] C. Mehlin, Structure-based drug discovery for Plasmodium falciparum, Comb. Chem. High Throughput Screen. 8 (2005) 5–14.

[16] R.L. Brady, A. Cameron, Structure-based approaches to the development of novel anti-malarials, Curr. Drug Targets 5 (2004) 137–149.

[17] R.T. Delfino, O.A. Santos-Filho, J.D. Figueroa-Villar, Molecular modeling of wild-type and antifolate resistant mutant Plasmodium falciparum DHFR, Biophys. Chem. 98 (2002) 287–300.

[18] S. Kamchonwongpaison, R. Quarrell, N. Charoensetakul, R. Ponsinet, T. Vilaivan, J. Vanichtanankul, W. Tarnchampoo, W. Sirawaraporn, G. Lowe, Y. Yuthavong, Inhibitors of multiple mutants of Plasmodium falciparum dihydrofolate reductase and their antimalarial activities, J. Med. Chem. 47 (2004) 673–680.

[19] S. Kamchonwongpaison, J. Vanichtanankul, B. Tarnchampoo, J. Yuvaniyama, S. Taweechai, Y. Yuthavong, Stoichiometric selection of tight-binding inhibitors by wild-type and mutant forms of malarial (Plasmodium falciparum) dihydrofolate reductase, Anal. Chem. 77 (2005) 1222–1227.

[20] M.D. Parenti, S. Pacchioni, A.M. Ferrari, G. Rastelli, Three-dimensional quantitative structure–activity relationship analysis of a set of Plasmodium falciparum dihydrofolate reductase inhibitors using a pharmacophore generation approach, J. Med. Chem. 47 (2004) 4258–4267.

[21] V.K. Agrawal, R. Sohgaura, P.V. Khadikar, QSAR studies on biological activity of piritrexim analogues against pc DHFR, Bioorg. Med. Chem. 10 (2002) 2919–2926.

[22] B.E. Mattioni, P.C. Jurs, Prediction of dihyrdrofolate reductase inhibition and selectivity using computational neural networks and linear discriminant analysis, J. Mol. Graph. Model. 21 (2003) 391–419.

[23] A. Gangjee, X. Lee, CoMFA and CoMSIA analyses of pneumocystis carinii dihydrofolate reductase, and rat liver dihydrofolate reductase, J. Med. Chem. (2005) 1448–1469.

[24] J.J. Sutherland, D.F. Weaver, Three-dimensional quantitative structure–activity and structure–selectivity relationships of dihydrofolate reductase inhibitors, J. Comput. Aided Drug Des. 18 (2004) 309–331.

[25] A. Ganjee, X. Lin, CoMFA and CoMSIA analyses of pneumocystis carinii dihydrofolate reductase, toxoplasma gondii dihydrofolate reductase, and rat liver dihydrofolate reductase, J. Med. Chem. 48 (2005) 1448–1469.

[26] O.A. Santos-Filho, A.J. Hopfinger, A Search for sources of drug resistance by the 4D-QSAR analysis of a set of anti-malarial dihydrofolate reductase inhibitors, J. Comput. Aided Mol. Des. 15 (2001) 1–12.

[27] T.-L. Chiu, S.-S. So, Development of neural network QSPR Models for hansch substituent constants. 2. Applications in QSAR studies of HIV-1 reverse transcriptase and dihydrofolate reductase inhibitors, J. Chem. Inf. Comput. Sci. 44 (2004) 154–160.

[28] S.Y. Hunt, C. Destering, G. Varani, D.P. Jacobus, G.A. Schiehser, H.-M. Shieh, I. Nevchas, J. Terpinski, C.H. Sibley, Identification of the optimal third generation antifolate against *P. falciparum* and *P. vivax*, Mol. Biochem. Parasitol. 144 (2005) 198–205.

[29] N. Guex, M.C. Peitsch, SWISS-MODEL and the Swiss-Pdbviewer: an environment for comparative protein modeling, Electrophoresis 18 (1997) 2714–2723.

[30] Molecular Operation Environment, MOE Molecular Operating Environment, Chemical Computing Group, Montreal, Quebec, Canada, 2005, Retrieved from http://www.chemcomp.com (January 4, 2007).

[31] G. Jones, P. Willett, R.C. Glen, A.R. Leach, R. Taylor, Development and validation of a genetic algorithm for flexible docking, J. Mol. Biol. 267 (1997) 727–748.

[32] Chemdraw, Cambridgesoft Inc., Cambridge, MA, 2007, Retrieved from http://www.camsoft.com 4/1/2007.

[33] T.A. Halgren, The merck force field, J. Comp. Chem. 17 (1996) 490–512.

[34] R. Thomsen, M.H. Christensen, MolDock: a new technique for high-accuracy molecular docking, J. Med. Chem. 49 (2006) 3315–3321.

[35] G.B., Fogel, M., Cheung, E., Pittman, D., Hecht, Modeling the inhibition of quadruple mutant *Plasmodium falciparum* dihydrofolate reductase by pyrimethamine derivatives, J. Comput. Aided Mol. Des. (2007), in press.

[36] C. Bissantz, G. Folkers, D. Rognan, Protein-based virtual screening of chemical databases, J. Med. Chem. 43 (2000) 4759–4767.

[37] R. Wang, L. Lai, S.J. Wang, Further development and validation of empirical scoring functions for structure-based binding affinity prediction, Comput. Aided Model. Des. 16 (2002) 11–26.